Applied Catalysis B: Environmental 160–161 (2014) 676–683

Contents lists available at ScienceDirect

Applied Catalysis B: Environmental

journal homepage: www.elsevier.com/locate/apcatb

Highly active electrocatalyst for oxygen reduction reaction from pyrolyzing carbon-supported iron tetraethylenepentamine complex

Hui-Juan Zhang*, Haoliang Li, Xiangtai Li, Shiyou Zheng, Bin Zhao, Junhe Yang*

School of Materials Science and Engineering, University of Shanghai for Science and Technology, Shanghai 200093, China

ARTICLE INFO

Article history:
Received 28 February 2014
Received in revised form 3 June 2014
Accepted 11 June 2014
Available online 20 June 2014

Keywords:
Oxygen reduction reaction
Non-precious metal catalyst
Iron
Tetraethylenepentamine
Nitrogen-doped

ABSTRACT

Development of non-precious metal catalysts for oxygen reduction reaction (ORR) is of great importance due to their significant potential application in energy converting and storing devices. In this work, a class of non-precious metal catalyst is prepared by using a simple and low-cost N_5 structure tetraethylenepentamine ligand, i.e. pyrolyzing iron tetraethylenepentamine chelate on carbon (FeTEPA/C) at 800 °C. The FeTEPA/C catalyst is characterized by transmission electron microscopy, Raman, X-ray diffraction, elemental analysis and X-ray photoelectron spectroscopy. It has been found that the unique FeTEPA/C catalyst contains 1.48 at% nitrogen and the absence of Fe-containing aggregates, and shows a higher catalytic activity towards the ORR than the commercial Pt/C catalyst either in acid or in alkaline electrolyte. Furthermore, a better ORR catalytic activity in terms of onset potential, peak potential, half-wave potential and limited-diffusing current is displayed in alkaline medium. The ORR on the FeTEPA/C catalyst follows a four-electron pathway among all the studied potential. The above superiorities make it a promising candidate for substituting the commercial Pt/C catalyst.

1. Introduction

Molecular oxygen (O_2) becomes a fascinating cathodic electrode for energy converting and storing devices, such as fuel cells and metal–air batteries, owing to its facile availability, natural abundance and environmental friendliness [1]. In fact, catalysts are required to reduce energy barrier of oxygen reduction reaction (ORR) in these renewable energy devices. Traditionally, platinum and platinum-based alloys have been considered as the most effective catalysts for the ORR [2]. For commercial applications, however, these catalysts are plagued by high cost, low abundance and poor durability of platinum metal. Therefore, developing non-precious metal catalysts to replace the platinum-containing catalysts for the ORR is the best option in terms of a long-term and sustainable solution.

Since Jahnke discovered the beneficial effect of heat treatment in an inert atmosphere to improve the catalytic activity and chemical stability [3], pyrolyzing the mixture of transition metal, carbon and nitrogen-containing precursors at high temperature have been extensively studied as the most promising non-precious metal catalysts for the ORR [4–10]. For example, polyaniline [4], di-polypyrrole [6], tetrasulfophthalocyanine [7], dicyandiamide [8], ethylenediamine [9] and tripyridyl triazine [10], together with Fe and/or Co salt were heat-treated to prepare the ORR catalysts.

Although there are numerous studies by various research groups in the world, the active sites of these catalysts are not clear and heavily debated in the literature [11–13]. However, there is an agreement on the requirement for preparing these non-precious metal catalysts for the ORR: (1) a transition metal, usually in the form of metal salts; (2) a nitrogen-containing source, such as porphyrins, polypyrrole, NH_3 and CH_3CN; (3) a source of carbon; and (4) heat treatment, usually at 800 °C. As far as the second point is concerned, the nitrogen-containing precursor can powerfully affect the catalytic activity and selectivity [4–10]. According to this, recently, we have studied a series of non-precious metal oxygen reduction catalysts, such as MTETA/C catalysts (carbon-supported transition metal triethylenetetramine chelate, M = Fe or Co) based on the small ring MN_4 structure [14,15], and CoDETA/C catalyst by using a N_3 structure diethylenetriamine ligand [16]. Till now, we have investigated the N_4 and N_3 structure nitrogen-containing ligands to prepare non-precious metal catalysts for the ORR, and how about the N_5 structure ligand?

Motivated by our curiosity, tetraethylenepentamine ($H_2NCH_2CH_2NHCH_2CH_2NHCH_2CH_2NH$ $CH_2CH_2NH_2$, TEPA), a simple and cheap N_5-structure ligand, is employed as the nitrogen precursor to develop highly active non-precious metal oxygen reduction catalyst (FeTEPA/C) in the present work. The FeTEPA/C

* Corresponding authors. Tel.: +86 21 5527 4065; fax: +86 21 5527 4065.
E-mail addresses: hjzhang@usst.edu.cn, 39395238@qq.com (H.-J. Zhang), jhyang@usst.edu.cn (J. Yang).

http://dx.doi.org/10.1016/j.apcatb.2014.06.014
0926-3373/

catalyst is subjected to a range of analytical techniques, including thermogravimetry (TGA), transmission electron microscopy (TEM), Raman, element analysis, X-ray diffraction (XRD) and X-ray photoelectron spectroscopy (XPS). Catalytic activities for the ORR are demonstrated by cyclic voltammograms (CVs) and rotating-ring disk electrode (RRDE) measurements in O_2-saturated acid and alkaline solutions at room temperature. The FeTEPA/C catalyst reported here has been optimized with respect to the ORR catalytic performance. This catalyst indeed exhibits an excellent ORR catalysis, outperforming the commercial carbon-supported Pt catalyst (20 wt% Pt/C, E-Tek) in alkaline and acidic mediums.

2. Experimental

2.1. Catalyst preparation

The preparation of FeTEPA/C catalyst was done in two steps: (i) modification of carbon support with hydrogen peroxide (H_2O_2) and (ii) synthesis of non-precious metal FeTEPA/C catalyst.

(i) Modification of carbon support with H_2O_2. 10.0 g commercially available carbon, namely Black Pearl 2000 (BP 2000) from Cabot Company, was ground in a planet-wheel agate mill with 100 g agate balls at 400 rpm for 2 h. The H_2O_2-oxidative treatment was achieved by mixing 10.0 g BP 2000 powder with 500 mL 30 wt% H_2O_2 solution under stirring condition for 24 h. The suspension was then filtered, washed with deionized water, dried in an oven at 80 °C, and finally ground to powder for further use.

(ii) Synthesis of non-precious metal FeTEPA/C catalyst. The structure illustration and schematic synthetic strategy of the FeTEPA/C catalyst are present in Fig. 1. TEPA, a simple N_5-structure ligand, can chelate with $FeCl_3$ to form the FeTEPA chelate easily, observed significant color changes in the experiment process. The structure of FeTEPA chelate molecular, which contains four five-membered rings, has been reported elsewhere [17]. In a typical synthesized method, 0.484 g inorganic iron (III) chloride hexahydrate ($FeCl_3{\cdot}6H_2O$) was dissolved in 50 mL ethanol at room temperature, showing orange-yellow solution in Fig. 1. Next, 1.0 mL tetraethylenepentamine (TEPA) was added into the above orange-yellow solution under stirring condition to form the FeTEPA chelate, displaying crimson solution in Fig. 1. Then 1.000 g the H_2O_2-treated BP 2000 was added to the chelate solution under stirring condition. Later, carbon-supported FeTEPA chelate suspension was stirred for 1 h and then dried to remove ethanol by a rotary evaporator at 50 °C under reduced pressure for 15 min. The resulting powder was pyrolyzed in high purity N_2 atmosphere at 800 °C for 90 min with a heating ramp of 5 °C min^{-1} from room temperature (25 °C). After that, the FeTEPA/C catalyst was ground to obtain fine powder product. The normal metal Fe loading with respect to carbon was kept at 10 wt%.

2.2. Working electrode preparation

A RRDE electrode (AFE7R9GCPT) consisting of a glassy carbon (GC) disk (5.61 mm diameter, a geometric surface area of 0.247 cm^2) surrounded by a Pt ring (6.25 mm inner diameter and 7.92 mm outer diameter) was purchased from Pine Instruments. For the working electrode preparation, this RRDE electrode was coated with FeTEPA/C catalyst ink to form the catalyst layer. The ink was prepared by ultrasonically dispersing 8 mg finely ground catalyst powder in 1.0 mL high purity water and 50 μL 5 wt% Nafion solution for 15 min. Then 15 μL of this ink was deposited onto the disk electrode surface to form a uniform layer. The overall catalyst loading was 486 μg cm^{-2} after air-drying. For comparison, commercial Pt/C catalyst (20 wt%, E-Tek) was also used to prepare the working electrode as mentioned above with the same catalyst loading of 486 μg cm^{-2}.

2.3. Electrochemical measurements

Electrochemical measurements were carried out on a bipotentiostat CHI 750D in a single-compartment conventional three-electrode cell filled with electrolyte at room temperature. In order to analog the operation condition of a polymer electrolyte membrane fuel cell and there is no significant difference in ORR testing of non-precious metal catalysts between H_2SO_4 and $HClO_4$ solutions [18], we chose H_2SO_4 as the acid electrolyte. The alkaline medium is KOH. A Pt mesh (10 mm × 10 mm) and a saturated calomel electrode (SCE) were used as the counter electrode and the reference electrode, respectively. The potential scan rate was fixed at 5 mV s^{-1} among all the electrochemical measurements.

Initially, the FeTEPA/C catalyst loaded on the GC disk was electrochemically stabilized by sweeping the CVs to remove any gaseous oxygen from the catalyst pores and fully wet the catalyst until steady CVs were obtained. To obtain the background capacitive currents, CVs were collected in N_2-saturated solution. Next, the solution was purged with O_2 and once again sweeping the potential until steady CVs were obtained. After that the CVs for the ORR tested were recorded in O_2-saturated solution. The net faradic current (or background correction) was obtained by subtracting the CVs in N_2-saturated solution from that obtained in O_2-saturated solution. For more quantitative measurements of the ORR activity, linear sweep voltammograms of the RRDE were obtained with the electrode rotated at 900 rpm. The ring potential was held at 1.0 and 0.5 V (*vs.* SCE) in acid and alkaline solutions, respectively. For comparison, commercial Pt/C catalyst (20 wt%, E-Tek) was examined at the same measurement conditions.

2.4. Calibration of the reference electrode

All potentials reported in this study hereinafter are referred with respect to the reversible hydrogen electrode (RHE). The calibration of SCE reference electrode was performed in a standard three-electrode system with polished Pt wires as the working and counter electrodes, and the SCE as the reference electrode. Electrolytes (0.1 M KOH and 0.5 M H_2SO_4) were pre-purged and saturated with high purity H_2, respectively. After steady, CVs was then run at a scan rate of 1 mV s^{-1}, and the average of the two potentials at which the current crossed zero was taken to be the thermodynamic potential for the hydrogen electrode reactions [19,20]. The calibration curves in alkaline and acid electrolytes are displayed in Fig. 2(a) and (b), respectively. According to these two figures, the correction formulas are as follows.

In 0.1 M KOH, $E(\mathrm{RHE}) = E(\mathrm{SCE}) + 1.013\,\mathrm{V}$.

In 0.5 M H_2SO_4, $E(RHE) = E(SCE) + 0.293\,\mathrm{V}$.

2.5. Physical characterizations

TGA of the FeTEPA/C catalyst precursor was performed on a Pyris 1 thermal analyzer (Perkin-Elmer) with the heating process from 50 to 900 °C at a rate of 5 °C min^{-1} in high purity N_2 atmosphere.

Raman spectrum was carried out in backscattering mode on the 400/400F dispersive Raman microscope spectrum (Perkin-Elmer) with a filter and a 785 nm laser. The laser beam was focused on the powder with a 50× lens, producing a spot (analysis area) of approximately 1–2 μm in diameter. The spectrum of FeTEPA/C catalyst was

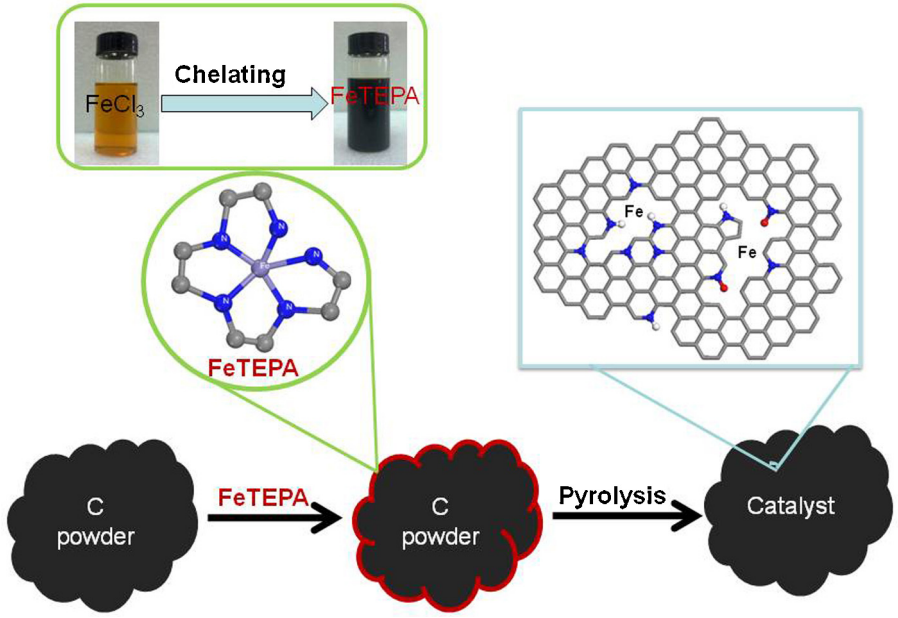

Fig. 1. Structural illustration and schematic synthetic strategy of the FeTEPA/C catalyst. The FeTEPA complex was synthesized via a chelating method that employed iron (III) chloride hexahydrate ($FeCl_3{\cdot}6H_2O$) as metal precursor and TEPA as the nitrogen source. Grey, blue, green, red, and white spheres represent C, N, Fe, O, and H, respectively. (For interpretation of the references to color in this figure legend, the reader is referred to the web version of the article.)

acquired by performing scans from 800 to 2000 cm^{-1} at a scan rate of 1 cm^{-1} with exposure time of 10 s and number of exposure of five times at 50% laser beam power energy. The spectrum was then analyzed by fitting the experimental data with four bands, using Origin 8 peak fitting.

CHNS/O Elemental Analyzer (2400 Series II, Perkin-Elmer) in the CHN mode and inductively coupled plasma emission spectrometer (ICP, Optima 7000DV, Perkin-Elmer) were applied to obtain the bulk compositions of C, N and Fe in the FeTEPA/C catalyst.

XRD was performed on an automated Rigaku diffractometer equipped with a Cu Kα radiation at a tube current of 20 mA and a tube potential of 40 kV. Data acquisition was recorded in the scanning angle range of 20–60° at a scan rate of 10° min^{-1}.

TEM was performed at a JEOL JEM-2010 operating at 200 keV. The FeTEPA/C catalyst was ultrasonically dispersed in absolute ethanol for 15 min. A small drop of the solution was then deposited onto a carbon-coated copper grid and left in air to dry.

XPS was carried out on a RBD upgraded PHI-5000C ESCA system (Perkin-Elmer) with a Mg Kα radiation ($h\nu$ = 1253.6 eV). The FeTEPA/C catalyst was directly pressed to a self-supported disk (10 × 10 mm) and mounted on a sample holder then transferred into analyzer chamber. A survey was performed from 1100 to 0 eV. The whole spectra and the narrow spectra of all elements with much high resolution were recorded by using RBD 147 interface (RBD Enterprises, USA) through the AugerScan 3.21 software. Binding energies were calibrated with the containment carbon (C 1s = 284.6 eV). Data analysis of C 1s, N 1s and O 1s was carried out by the XPSPeak4.1 program with a fixed Gaussian–Lorentzian mix function (Gaussian 80%) and a Shirley-type background subtraction. The full width at half-maximum (FWHM) values was fixed at 1.2 eV for all the peaks during fitting. All the fitted peaks of the deconvoluted spectra were self-consistent, allowing quantitative comparisons.

3. Results and discussion

TGA curve (black line) of FeTEPA/C catalyst precursor is shown in Fig. 3. In order to clarify the major mass loss temperatures, DTG (derivative thermogravimetric) curve (blue line) is also depicted. According to the DTG curve, there are mainly three steps on the TGA curve. The first step starts at 50 °C and reaches a plateau near 230 °C, which can be assigned to the volatilization of TEPA ligand on the carbon surface. The second step is from 230 to 527 °C corresponding to the degradation of FeTEPA chelates and loss of its volatile

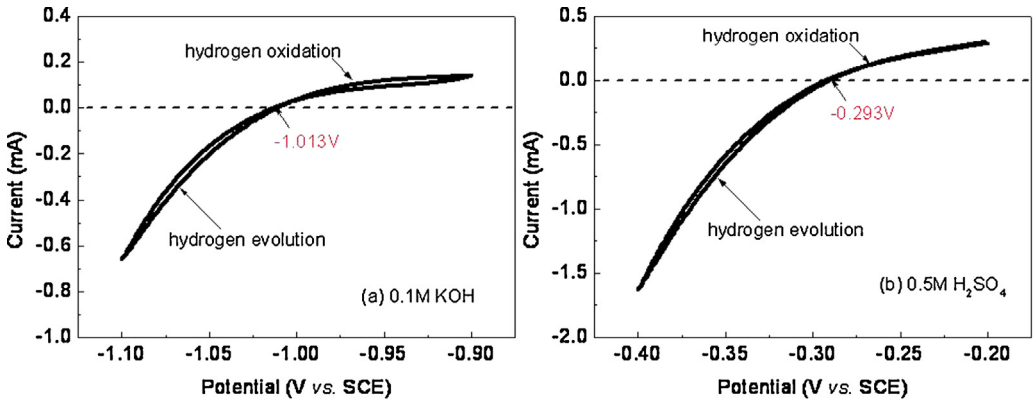

Fig. 2. The potential calibration curves carried in (a) 0.1 M KOH and (b) 0.5 M H_2SO_4.

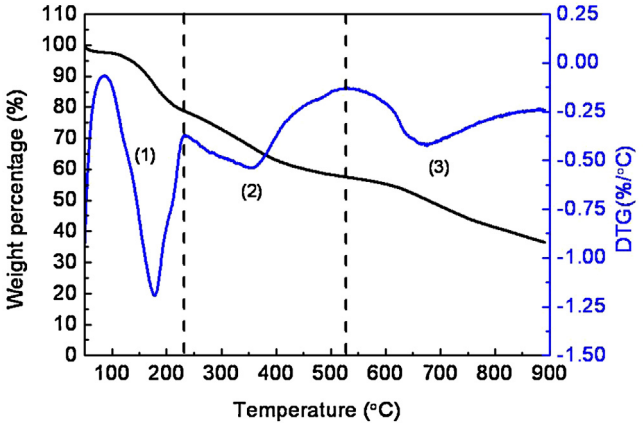

Fig. 3. TGA/DTG curves of the FeTEPA/C catalyst precursor performed at a heating rate of 5 °C min^{-1} under a flowing high purity N_2 with its flow rate of 20 mL min^{-1}.

fragments. The last step starts at 527 °C and ends at 900 °C, which indicates the decomposition of FeTEPA chelates. Similar studies have also investigated for catalyst precursors of FeTETA/C [15], CoDETA/C [16] and CoTETA/C [21].

Raman spectrum of FeTEPA/C catalyst, as shown in Fig. 4, is deconvoluted into four peaks. There are two main characteristic peaks: the D band around 1300 cm^{-1} which is attributed to the presence of disordered amorphous carbon due to an A_{1g} vibrational mode and the G band at 1592 cm^{-1} which is associated with a splitting of the E_{2g} stretching mode of graphite and the structural intensity of the sp^2-hybridized carbon atoms. As displayed in Fig. 4, two additional broad peaks, concealed by the G and D bands, are required to accurately fit the experimental Raman spectra. According to the literature [22], these two additional bands are attributed to amorphous carbon (A_m band, 1400–1480 cm^{-1}) and sp^3 carbon (P band, 1140–1190 cm^{-1}), respectively. Relative intensity ratio of D- to G-band (I_D/I_G) after fitting gives qualitative information of defects degree. The I_D/I_G value for the FeTEPA/C catalyst is 1.26. Ratio of the full widths at half maxima of D and G peaks, w_D/w_G, is also taken as a measure of the disorder in the catalyst [22]. Based on this, it is 1.29 for FeTEPA/C catalyst.

XPS survey spectrum and surface element compositions (at%) of the FeTEPA/C catalyst are given in Fig. 5(a). It clearly shows a predominant C 1s peak at about 285.6 eV, an O 1s peak around 533 eV, a weak peak N 1s at 400 eV and a much weaker Fe 2p peak at 714 eV. It also indicates that this non-precious metal catalyst is composed of C, O, N and Fe with a content order as C > O > N > Fe. Quantitative XPS analysis shows that carbon is present around 88%, oxygen

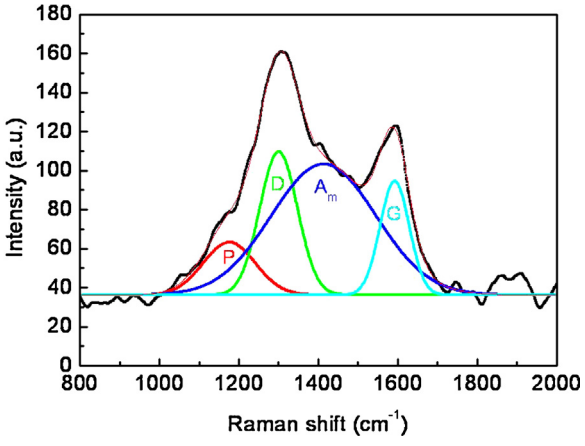

Fig. 4. Raman spectrum with fittings of the FeTEPA/C catalyst.

about 9.67%, nitrogen is 1.48% and iron near 0.15% on the catalyst surface. This means that larger electronegative atoms nitrogen (electronegativity: 3.04) and oxygen (3.55) with respect to carbon (electronegativity: 2.55) are doped in carbon matrix and creating of positive charge density on the adjacent C atoms, which is favorable for adsorption molecular oxygen and catalyzing it reduction [23]. In particular, doped-nitrogen cause structural deformation of carbon and it increases the n-type conductivity by acting as an electron donor and also induces charge delocalization for adjacent carbon atoms due to its strong electron affinity [5]. On the other hand, the carbon content is around 70 wt% and nitrogen is about 1.20 wt% measured by Elemental Analyzer (2400 Series II), the iron content is 1.56 wt% measured by ICP. Differences of these two results can be attributed to the detection scopes of these two measurements: the depth of XPS scanning is only 3–6 nm, which is used to analysis element content on catalyst's surface, however, Elemental Analyzer and ICP are used to analyze element content on the whole catalyst. Furthermore, XPS result is a form of atomic ratio (at%), while C and N element analysis is in a mass ratio (wt%).

High-resolution XPS spectrum of C 1s for the FeTEPA/C catalyst is displayed in Fig. 5(b). We can see that a predominant C 1s peak at a higher binding energy of about 285.6 eV as compared to the value of carbon black 284.6 eV and the binding energy shoulder is also wider when compared to carbon black [12]. This can be attributed to the interaction of carbon with nitrogen and oxygen on carbon surface. When some carbon atoms are adjacent to nitrogen and oxygen atoms in carbon matrix, these carbon atoms will inherently have a higher C 1s binding energy since N 1s and O 1s usually show higher binding energy of 396–408 and 528–540 eV, respectively [12]. The strong interaction between carbon atom and nitrogen/oxygen atom also contributes to a wider C 1s peak and a binding energy shoulder. Close observation of C 1s reveals seven peaks at 284.75, 285.47, 286.25, 286.97, 287.71, 288.76 and 289.89 eV, which can be assigned to the carbon component in C═C, C—C, C—O, C—N, C═O, —COO and O—COO, respectively [18].

High-resolution XPS spectrum of N 1s for the FeTEPA/C catalyst is displayed in Fig. 5(c). Based on the literature [20], peaks of N 1s at 397–399.5, 399–400.5, 400.2–400.9, 401–403 and 402–405 eV can be assigned to pyridinic-N, nitrile or Me-N_x, pyrrolic-N, graphitic-N and oxidized-N, respectively. Among these five nitrogen functional groups, pyridinic-N refers to the nitrogen atom on the edge of graphite planes with two adjacent carbon atoms. It has one lone pair of electrons in addition to the one electron donated to the conjugated bond system, imparting Lewis basicity to the carbon [12]. Graphitic-N, which is also termed as "quaternary-N", represents the nitrogen atom bonded to three carbon atoms within a graphite (basal) plane, while pyrrolic groups refer to nitrogen atoms that contribute to the π system with two p electrons [12]. As shown in Fig. 5(c), these five nitrogen functional groups are all present in the FeTEPA/C catalyst with its content order of nitrile or Me-N_x ≈ pyrrolic-N > graphitic-N > pyridinic-N > oxidized-N.

Fig. 5(d) shows the high-resolution XPS spectrum of O 1s on the FeTEPA/C catalyst surface. As illustrated in Fig. 5(d), various oxygen species are present: (1) oxygen with the peaks at 532 and 532.9 eV is associated mostly with carbon and possibly nitrogen, (2) oxygen is in carbonate and nitrate-like species with the peaks at 534 and 535 eV, and (3) oxygen is from adsorbed water with the peaks at 534–537 eV [24]. The high oxygen loading observed on the catalyst may partly be the physical adsorption of molecular oxygen. Furthermore, L. Dai's group reported that the O peaks arose, most probably, from the incorporation of physicochemically adsorbed molecular oxygen, which was suggested to be advantageous for ORR application [23].

Fig. 6(a) shows the XPS spectrum of Fe $2p_{3/2}$ and $2p_{1/2}$ on the FeTEPA/C catalyst surface. Peaks at 711 eV for Fe $2p_{3/2}$ and 725 eV for Fe $2p_{1/2}$ are observed, although the signal-to-noise

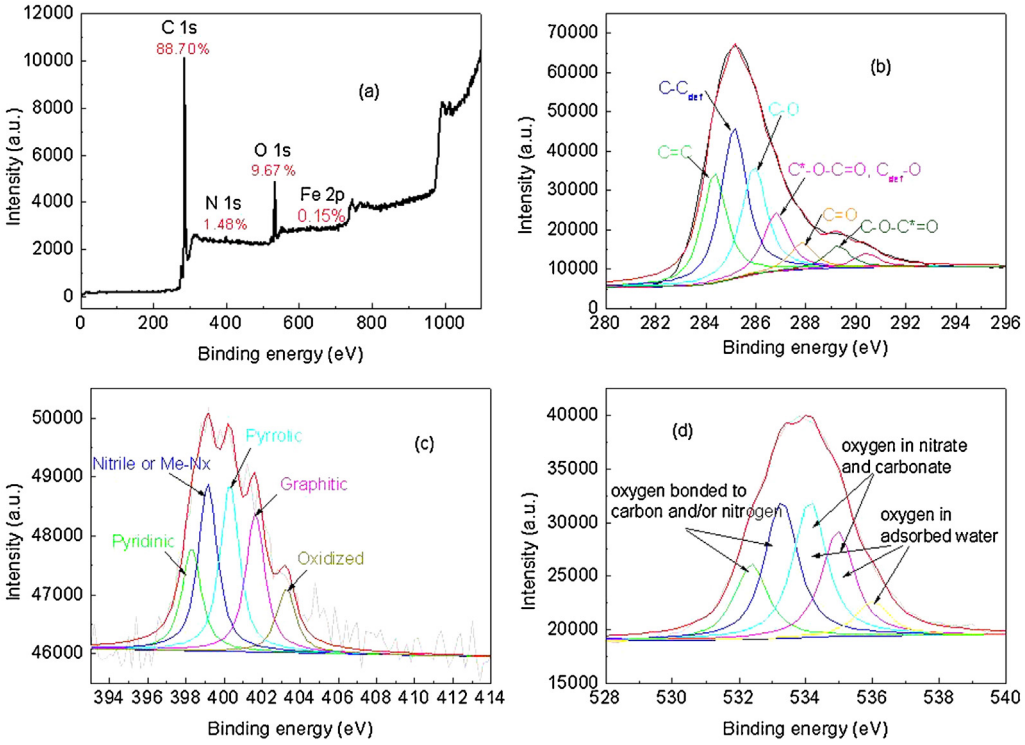

Fig. 5. (a) XPS survey spectrum, high-resolution XPS spectra of (b) C 1s, (c) N 1s and (d) O 1s in the FeTEPA/C catalyst.

ratio for the Fe 2p peaks is poor due to the low Fe content of 0.15%. The peak at 711 eV is attributed to Fe(III) according to the value of 710.8–711.8 eV reported in the literature [25]. Others reported that the peak of Fe $2p_{3/2}$ in heat-treated iron phthalocyanines and iron porphyrins adsorbed on carbon black shifted to a lower binding energy due to the formation of aggregates including Fe(0) (706.7–707.2 eV), Fe(II) (707.1–708.7 eV) or Fe carbides (706.7–706.9 eV), and a similar peak shift for Fe $2p_{1/2}$ according to the binding energy: Fe(III), 725.1 eV; Fe(II), 722.9 eV; Fe(0), 719.7 eV [26,27]. Therefore, the results in the present study free of these peak

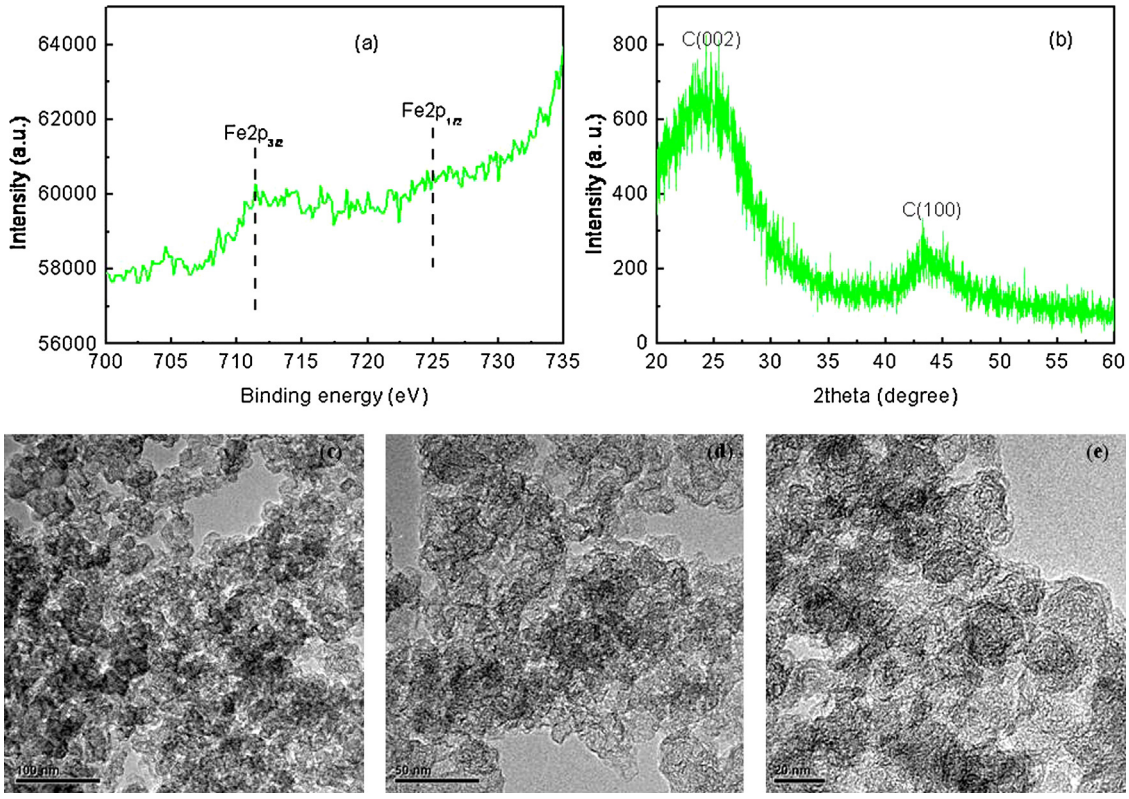

Fig. 6. (a) High-resolution XPS spectrum of Fe 2p, (b) XRD, and TEM images with the scale bars (c) 100 nm, (d) 50 nm, and (e) 20 nm of the FeTEPA/C catalyst.

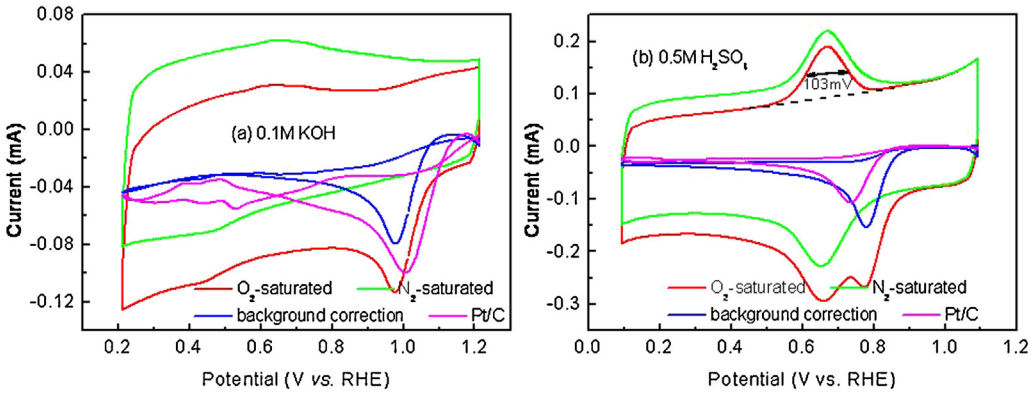

Fig. 7. CVs for oxygen reduction at the FeTEPA/C catalyst in the O_2-saturated (red lines) and N_2-saturated (green lines) (a) 0.1 M KOH and (b) 0.5 M H_2SO_4 at a potential scan rate of 5 mV s^{-1}. The blue lines are their CVs after the background collection. The CVs of commercial Pt/C catalyst after the background collection (pink lines) in both two electrolytes are also shown for comparison.(For interpretation of the references to color in this figure legend, the reader is referred to the web version of the article.)

shifts indicated the absence of any aggregates. Furthermore, the absence of the Fe-containing aggregates is also suggested by the XRD spectrum as shown in Fig. 6(b). The broad peaks at $2\theta = 25^\circ$ and 44° are attributed to amorphous carbon, usually observed for activated carbon [25]. There is no peak attributable to the crystalline particles, especially between 40° and 55° where the peaks attributed to the Fe aggregates are reported to appear [25]. As shown the TEM images of the FeTEPA/C catalyst in Fig. 6(c)–(e), observation of the amorphous carbon part is performed in the thin gray area, which also suggests the absence of the Fe aggregates [25].

Typical CVs of FeTEPA/C catalyst tested in O_2-saturated (red line) and N_2-saturated (green line) 0.1 M KOH are displayed in Fig. 7(a). For comparison, the CVs after the background correction of FeTEPA/C catalyst (blue line) and commercial Pt/C catalyst (pink line) are also shown in Fig. 7(a). For FeTEPA/C catalyst, compared with the featureless CVs obtained in N_2-saturated solution, the CVs tested in O_2-saturated solution show a well-defined cathodic ORR peak, indicating the obvious catalytic activity of FeTEPA/C catalyst in alkaline solution. Concretely, the ORR peak potential (E_p) is 0.978 V and current (I_p) is −0.080 mA after the background correction, although showing a slight negative than that of Pt/C catalyst with the E_p of 1.007 V and I_p at −0.1 mA. However, the E_p shifts to a higher value, as compared to the Fe_3O_4/N-GAs (−0.34 V *vs.* Ag/AgCl) [28]. Furthermore, it also displays a better E_p than the CoDETA/C-N_2 (0.914 V), CoDETA/C-Ar (0.891 V) and CoDETA/C-CO_2 (0.888 V) reported in our group recently [16]. Here, we can know that FeTEPA/C catalyst has a good ORR catalytic activity in alkaline electrolyte.

Fig. 7(b) shows typical CVs of FeTEPA/C catalyst measured in O_2-saturated (red line) and N_2-saturated (green line) 0.5 M H_2SO_4, along with its CVs after the background correction (blue line). The CVs of commercial Pt/C catalyst after background correction (pink line) is also shown in Fig. 7(b) for comparison. The CVs tested in O_2-saturated solution show a well-defined cathodic ORR peak with the E_p of 0.787 V and the I_p as −0.092 mA after the background correction, indicating the obvious catalytic activity of FeTEPA/C catalyst in acid solution. An obvious positive shift of E_p is displayed, as compared to the reported values for CoDETA/C-N_2 (0.767 V), CoDETA/C-Ar (0.762 V) and CoDETA/C-CO_2 (0.690 V) in acid solution [16]. Another significant feature is a pair of well-developed redox peaks at *ca.* 0.67 V. The half-height width of this peak is *ca.* 103 mV, very close to the theoretical value of 96 mV, expected for a reversible one-electron process involving surface species [4]. There are two surface processes that can possibly give rise to the observed redox behavior in this case: (i) one-electron reduction/oxidation of the surface quinone-hydroquinone groups and (ii) Fe^{3+}/Fe^{2+} reduction/oxidation [4]. Here, this well-developed redox peaks situated around 0.67 V belongs to the latter. P. Zelenay's group also obtained this reversible CV feature of the PANI-Fe-C catalyst by using an *in situ* electrochemical X-ray absorption study of the PANI-Fe-C system experiment [4].

Current–potential curves of FeTEPA/C catalyst and commercial Pt/C catalyst measured in 0.1 M KOH and 0.5 M H_2SO_4 are compared in Fig. 8. It demonstrates a single-step wide platform, indicating a four-electron ORR process [4,5,16]. Among all the studied potential, a trend of catalytic activity for FeTEPA/C catalyst in alkaline solution is better than that in acid solution, in terms of the ORR onset potential, half-wave potential and the diffusion-limiting current. An exciting phenomenon is that the FeTEPA/C catalyst has better catalytic activity than commercial Pt/C catalyst in both two electrolytes. For example, as displayed in Fig. 8, at the current of −0.6 mA, the potentials of FeTEPA/C catalyst are higher than that of Pt/C catalyst with 40 mV and 47 mV in alkaline and acid mediums, respectively. Furthermore, its ORR onset potential in alkaline solution appears obvious positive as compared to the reported values for Fe_3O_4/N-GAs (−0.19 V *vs.* Ag/AgCl), Fe_3O_4/N-GSs (−0.26 V *vs.* Ag/AgCl) and Fe_3O_4/N-CB (−0.24 V *vs.* Ag/AgCl) with the scan rate of 100 mV s^{-1} [28]. There are also obvious positive shifts in comparison with Co_3O_4/rmGO (0.88 V, 0.1 M KOH) at the same scan

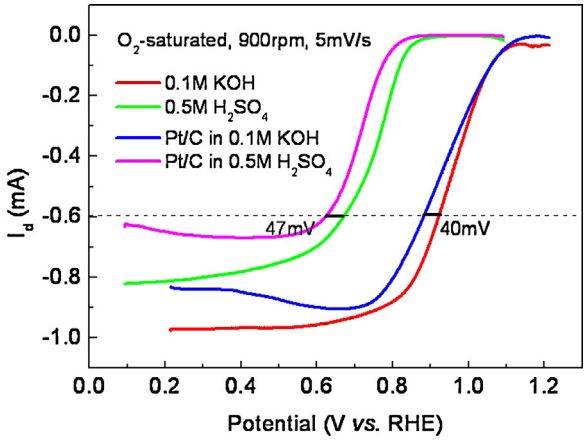

Fig. 8. Polarization curves for oxygen reduction at the FeTEPA/C catalyst measured in O_2-saturated 0.1 M KOH (red line) and 0.5 M H_2SO_4 (green line). For all RRDE measurements, the catalyst loadings were 486 μg cm^{-2}. The electrode rotation speed was 900 rpm and the scan rate was 5 mV s^{-1}. The polarization curves of commercial Pt/C catalyst tested at the same catalyst loading in O_2-saturated 0.1 M KOH (blue line) and 0.5 M H_2SO_4 (pink line) are also shown for comparison.(For interpretation of the references to color in this figure legend, the reader is referred to the web version of the article.)

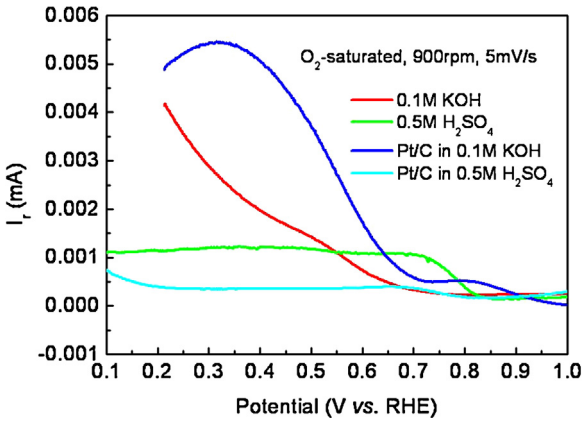

Fig. 9. The ring current as a function of the disk potential at the FeTEPA/C catalyst measured in O_2-saturated 0.1 M KOH (red line) and 0.5 M H_2SO_4 (green line) at a potential scan rate of 5 mV s^{-1} and a rotation rate of 900 rpm. The Pt ring electrode was poised at 0.5 V (*vs.* SCE) in 0.1 M KOH and 1.0 V (*vs.* SCE) in 0.5 M H_2SO_4. The ring currents of commercial Pt/C catalyst measured at the same catalyst loading are also shown for comparison.(For interpretation of the references to color in this figure legend, the reader is referred to the web version of the article.)

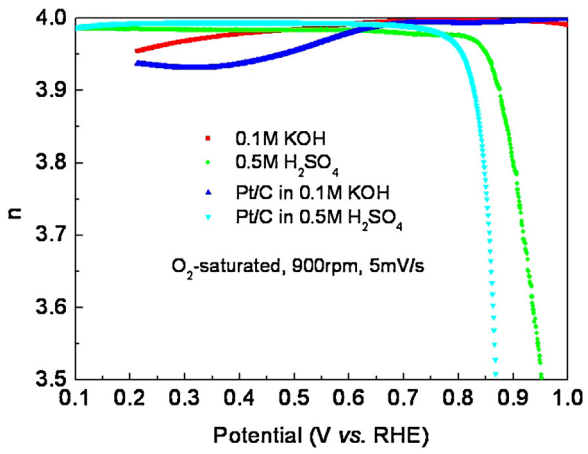

Fig. 10. The number of electrons transferred per molecule oxygen at the FeTEPA/C catalyst in 0.1 M KOH (red square) and 0.5 M H_2SO_4 (green rhombus). The data of commercial Pt/C catalyst in these electrolytes are also shown for comparison.(For interpretation of the references to color in this figure legend, the reader is referred to the web version of the article.)

rate [19]. Well-defined diffusion-limiting current plateaus are displayed and the polarization curves exhibit typical S-shape in these two electrolytes. This means that ORR on the FeTEPA/C catalyst is fast enough and the reaction happens only on the outer part of the catalyst, then a flat limiting current plateau is observed. It indicates that FeTEPA/C catalyst has a good catalytic activity in alkaline and acid electrolytes.

Fig. 9 gives the ring current as a function of the disk potential for the ORR on FeTEPA/C catalyst and commercial Pt/C catalyst measured in 0.1 M KOH and 0.5 M H_2SO_4 at a potential scan rate of 5 mV s^{-1}. We can see that the ring currents initiate at 0.943 V in alkaline solution and 0.843 V in acid solution, indicating that the generation of peroxide is taking place and the disk potential-dependent selectivity appears. In 0.1 M KOH, the ring currents of FeTEPA/C catalyst are less than that of commercial Pt/C catalyst among all the studied potential, which suggests that FeTEPA/C catalyst has a better four-electron-reduction selectivity for the ORR. On the other hand, in 0.5 M H_2SO_4, the ring currents of FeTEPA/C catalyst are higher than that of Pt/C catalyst and these two curves show the same shape. An interesting feature is the shape of the ring current as a function of the disk potential for FeTEPA/C catalyst in these two electrolytes: in alkaline solution, the ring current increases monotonously along with the disk potential decreases, while in acid solution, the ring current keeps unchanged when the disk potential lower than 0.7 V.

Generally, there are two possible parallel reactions for the ORR: one is a 2e mechanism to generate the intermediate H_2O_2 with its further reduction or its decomposition, and the other is a 4e path to generate H_2O (an ideal ORR). The number of electrons transferred per molecular oxygen (n) and the percentage of H_2O_2 ($\%H_2O_2$) or HO_2^- ($\%HO_2^-$) produced in acid and alkaline solutions can be determined by the following equations [4,6,23].

$$n = \frac{4I_d}{(I_d + I_r/N)} \quad (1)$$

$$\%H_2O_2\,(\text{or}\,\%HO_2^-) = \frac{100(4-n)}{2} \quad (2)$$

where I_d is the faradic current at the disk, I_r is the faradic current at the ring, and N is the RRDE collection efficiency as 0.37.

An n value of 4.0 is equivalent to 100% selectivity towards water formation, while an n value of 2.0 is equivalent to 100% selectivity towards peroxide formation. Fig. 10 illustrates the n calculated from the RRDE experimental data for FeTEPA/C catalyst in alkaline and acid solutions, respectively. For comparison, the data of commercial Pt/C catalyst are also shown. On the whole, the n changes between 3.9 and 4.0 among the disk studied potential, which clearly indicates that the catalytic ORR on FeTEPA/C catalyst surface in these two mediums becomes predominantly 4e reaction, leading to the production of water. Furthermore, the 4e reaction selectivity of FeTEPA/C catalyst is similar to that of commercial Pt/C catalyst. In alkaline solution, along with the disk potential decreases, the n decreases slightly. This situation does not appear in acid solution. The corresponding $\%H_2O_2$ (or $\%HO_2^-$) displayed in Fig. 11 further indicates that the 4e reduction to water is predominated for FeTEPA/C catalyst in alkaline and acid mediums. In these two solutions, its $\%H_2O_2$ (or $\%HO_2^-$) is less than 5% among all the disk potentials studied. By the way, the $\%HO_2^-$ for FeTEPA/C catalyst is less than Co_3O_4/rmGO (below 12%, 0.1 M KOH) [19].

In order to accelerate the future development of the FeTEPA/C catalyst, it is essential to well understand and elucidate its active sites. As for the active site in the FeTEPA/C catalyst studied in the

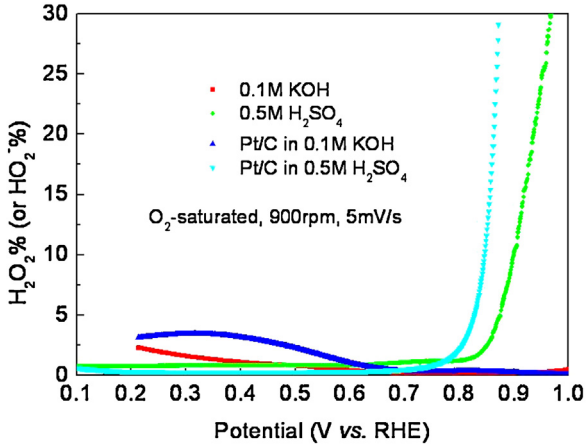

Fig. 11. The percentage of peroxide ($\%HO_2^-$ and $\%H_2O_2$) at the FeTEPA/C catalyst in 0.1 M KOH (red square) and 0.5 M H_2SO_4 (green rhombus). The $\%HO_2^-$ and $\%H_2O_2$ for commercial Pt/C catalyst in these catalysts are also shown for comparison.(For interpretation of the references to color in this figure legend, the reader is referred to the web version of the article.)

present work, we believe that the transition metal Fe is just served as a catalyst to prompt the incorporation of electron-accepting nitrogen atoms in the conjugated carbon plane and the significantly high ORR activity comes from the net positive charge on carbon atoms created by the nitrogen dopants of a higher electronegativity than that of carbon [13,29–33]. Many other researchers also get similar conclusion. For example, Kobayashi's group reported that light elements such as C and N were components of the ORR active sites in the FePc/C catalyst pyrolyzed at high temperature where the FeN_4 structure in the macrocycle was mostly decomposed [29]. They also believed that the residual Fe itself did not seem to contribute directly to the ORR activity as the oxygen reduction potential was approximately unchanged by the acid washing [29]. Similarly, Oh and Kim also indicated that the transition metal Fe itself did not behave as an active site for ORR, while the total nitrogen content and the active nitrogen functional groups, such as pyridinic-N and graphitic-N, were strongly dependent on the type of transition metal and the amount of transition metal used [13]. They believed that transition metals served to catalyze the formation of active nitrogen functional groups for the ORR by doping nitrogen into carbon [13]. Ozkan's group has found that the existence of the catalytic active site in CN*x* did not depend on the transition metal Fe [30]. Recently, Cheon et al. have revealed a weakening of the interaction between oxygen atom and FeCo-OMPC, which appeared responsible for its significantly high ORR activity [31]. Dai's group indicated that the nitrogen-induced charge delocalization could change the chemisorptions mode of O_2 from the usual end-on adsorption (Pauling model) at the CCNT surface to a side-on adsorption (Yeager model) onto the NCNT electrodes, which could effectively weaken the O–O bonding to facilitate ORR at the NCNT/GC electrodes [32,33].

4. Conclusions

In summary, a class of promising non-precious metal catalyst for the ORR has been prepared based on pyrolyzing iron tetraethylenepentamine chelate on carbon (FeTEPA/C) at 800 °C in high purity N_2 atmosphere. Physical characteristic measured by TEM, XRD and XPS demonstrate the nitrogen-doped intro carbon matrix with 1.48 at% and a low Fe of 0.15 at%. The absence of Fe-containing aggregates is also suggested. The ORR examined on FeTEPA/C-modified glassy carbon electrode shows that the FeTEPA/C catalyst has a higher catalytic activity and selectivity to water towards the ORR in acid and alkaline electrolytes, as compared to the commercial Pt/C catalyst. Furthermore, it displays a better catalytic activity and selectivity to water in alkaline than that in acid in terms of the peak potential, onset potential, half-wave potential and limited-diffusing current. The ORR peak potential of FeTEPA/C catalyst in alkaline is 0.978 V, while in acid, it is 0.787 V. The ORR on the FeTEPA/C catalyst proceeds nearly through a 4e reaction among the potential we studied in these two solutions with the number of electrons transferred changes between 3.9 and 4.0. The above superiorities make it a promising candidate for substituting the commercial Pt/C catalyst.

Acknowledgments

The authors are grateful for the financial support of this work by the National Science Foundation of China (51102167, 51102169 and 51272157), Key Basic Research of Shanghai Science and Technology Program (12JC1406900), Shanghai Science and Technology Program (13ZR1429000).

References

[1] X. Fu, Y. Liu, X. Cao, J. Jin, Q. Liu, J. Zhang, Appl. Catal. B: Environ. 130–131 (2013) 143–151.
[2] J. Zhang, K. Sasaki, E. Sutter, R.R. Adzic, Science 12 (2007) 220–222.
[3] H. Jahnke, M. Schönborn, G. Zimmermann, Top. Curr. Chem. 61 (1976) 133–181.
[4] G. Wu, K.L. More, C.M. Johnston, P. Zelenay, Science 332 (2011) 443–447.
[5] C.H. Choi, S.H. Park, S.I. Woo, Appl. Catal. B: Environ. 119–120 (2012) 123–131.
[6] J. Masa, A. Zhao, W. Xia, M. Muhler, W. Schuhmann, Electrochem. Acta 128 (2014) 271–278.
[7] X. Gao, J. Wang, Z. Ma, J. Ye, Electrochem. Acta 130 (2014) 543–550.
[8] M. Vikkisk, I. Kruusenberg, U. Joost, E. Shulga, I. Kink, K. Tammeveski, Appl. Catal. B: Environ. 147 (2014) 369–376.
[9] X. Li, B.N. Popov, T. Kawahara, H. Yanagi, J. Power Sources 196 (2011) 1717–1722.
[10] S. Li, L. Zhang, H. Liu, M. Pan, L. Zan, J. Zhang, Electrochim. Acta 55 (2010) 4403–4411.
[11] M. Lefèvre, J.P. Dodelet, P. Bertrand, J. Phys. Chem. B 106 (2002) 8705–8713.
[12] N.P. Subramanian, X. Li, V. Nallathambi, S.P. Kumaraguru, H. Colon-Mercado, G. Wu, J.W. Lee, B.N. Popov, J. Power Sources 188 (2009) 38–44.
[13] H. Oh, H. Kim, J. Power Sources 212 (2012) 220–225.
[14] H.J. Zhang, X. Yuan, W. Wen, D.Y. Zhang, L. Sun, Q.Z. Jiang, Z.F. Ma, Electrochem. Commun. 11 (2009) 206–208.
[15] H.J. Zhang, X. Yuan, Z. Wang, J. Yang, Z.F. Ma, Electrochim. Acta 87 (2013) 599–605.
[16] H.J. Zhang, H. Li, X. Li, H. Qiu, X. Yuan, B. Zhao, Z.F. Ma, J. Yang, Int. J. Hydrogen Energy 39 (2014) 267–276.
[17] N. Pienack, S. Lehmann, H. Lühmann, M. El-Madani, C. Näther, W. Bensch, Z. Anorg. Allg. Chem. 634 (2008) 2323–2329.
[18] F. Jaouen, J. Herranz, M. Lefèvre, J.P. Dodelet, U.I. Kramm, I. Herrmann, P. Bogdanoff, J. Maruyama, T. Nagaoka, A. Garsuch, J.R. Dahn, T. Olson, S. Pylypenko, P. Atanassov, E.A. Ustinov, Appl. Mater. Interf. 1 (2009) 1623–1639.
[19] Y. Liang, Y. Li, H. Wang, J. Zhou, J. Wang, T. Regier, H. Dai, Nat. Mater. 10 (2011) 780–786.
[20] Y. Liang, H. Wang, P. Diao, W. Chang, G. Hong, Y. Li, M. Gong, L. Xie, J. Zhou, J. Wang, T.Z. Regier, F. Wei, H. Dai, J. Am. Chem. Soc. 134 (2012) 15849–15857.
[21] H.J. Zhang, Q.Z. Jiang, L. Sun, X. Yuan, Z.F. Ma, Electrochim. Acta 55 (2010) 1107–1112.
[22] F. Charreteur, F. Jaouen, S. Ruggeri, J.P. Dodelet, Electrochim. Acta 53 (2008) 2925–2938.
[23] S. Wang, E. Iyyamperumal, A. Roy, Y. Xue, D. Yu, L. Dai, Angew. Chem. Int. Ed. 50 (2011) 11756–11760.
[24] I. Kruusenberg, L. Matisen, Q. Shah, A.M. Kannan, K. Tammeveski, Int. J. Hydrogen Energy 37 (2012) 4406–4412.
[25] J. Maruyama, I. Abe, Chem. Mater. 18 (2006) 1303–1311.
[26] G. Lalande, G. Faubert, R. Côté, D. Guay, J.P. Dodelet, L.T. Weng, P. Bertrand, J. Power Sources 61 (1996) 227–237.
[27] G. Faubert, R. Côté, D. Guay, J.P. Dodelet, G. Denes, P. Bertrand, Electrochim. Acta 43 (1998) 341–353.
[28] Z.S. Wu, S. Yang, Y. Sun, K. Parvez, X. Feng, K. Müllen, J. Am. Chem. Soc. 134 (2012) 9082–9085.
[29] M. Kobayashi, H. Niwa, M. Saito, Y. Harada, M. Oshima, H. Ofuchi, K. Terakura, T. Ikeda, Y. Koshigoe, J. Ozaki, S. Miyata, Electrochim. Acta 74 (2012) 254–259.
[30] D. von Deak, D. Singh, E.J. Biddinger, J.C. King, B. Bayram, J.T. Miller, U.S. Ozkan, J. Catal. 285 (2012) 145–151.
[31] J.Y. Cheon, T. Kim, Yn. Choi, H.Y. Jeong, M.G. Kim, Y.J. Sa, J. Kim, Z. Lee, T.-H. Yang, K. Kwon, O. Terasaki, G.-G. Park, R.R. Adzic, S.H. Joo, Sci. Rep. 3 (2013) 2715, http://dx.doi.org/10.1038/srep02715.
[32] K. Gong, F. Du, Z.H. Xia, M. Durstock, L. Dai, Science 323 (2009) 760–764.
[33] D. Yu, Y. Xue, L. Dai, J. Phys. Chem. Lett. 3 (2012) 2863–2870.